Available online at www.sciencedirect.com
ScienceDirect
International Journal of Thermal Sciences 46 (2007) 856–868
International Journal of Thermal Sciences
www.elsevier.com/locate/ijts

Numerical simulation of a water spray—Radiation attenuation related to spray dynamics

A. Collin, P. Boulet *, G. Parent, D. Lacroix

Laboratoire d'Energétique et de Mécanique Théorique & Appliquée (LEMTA), CNRS UMR 7563, Université Henri Poincaré, Nancy 1, Faculté des Sciences et Techniques BP 239, 54506 Vandoeuvre cedex, France

Received 8 March 2006; received in revised form 18 October 2006; accepted 10 November 2006

Available online 14 December 2006

Abstract

Radiation attenuation by a water spray is predicted on the basis of a detailed simulation. First of all, a two-way coupling treatment of the spray dynamics is achieved through an Eulerian–Lagrangian modeling. Droplet distribution combined with water vapor and carbon dioxide volume fractions are then used to compute the radiative properties of the medium. A simulation of radiation propagation is performed, aimed at the computation of the spectral transmittance through the spray. A Monte Carlo technique is used to describe radiation absorption and scattering phenomena for a real droplet polydispersion and an equivalent monodispersion. Numerical results of spray attenuation are compared to experimental data obtained on a laboratory spray with low flow rate. Satisfying accuracy can be obtained for the numerical prediction if a realistic size distribution is used for the pulverization. The mean Sauter diameter and the volumetric fraction of droplets are found to vary with the position in the spray. Tentative predictions with a monodispersion therefore fail in predicting the attenuation ability of the spray at various vertical positions below the injection point.

Keywords: Droplet; Two-phase flow; Eulerian; Lagrangian; Transmittance; Radiative transfer

1. Introduction

Water sprays are usual tools used in fire safety devices. Our focus here, is on one peculiar application: the use of spray curtains as radiative shields. No direct interactions are considered between flames and droplets, the curtain is created outside of the fire and its action is only devoted to radiation attenuation in order to protect a given target. Applications of such devices may be found in the frame of any plant where flammable products are stored to avoid hazardous fire propagation from tank to tank in the case of an accident. A similar use of water curtains could concern high temperature processes if consecutive strong radiation emissions have to be mitigated. Such a goal may be reached owing to absorbing and scattering abilities of water sprays. This behavior has been demonstrated among others through the results of the ASTRRE project in the late 90's. See for example the former studies reported in Prétrel and Buchlin [1], Dembélé et al. [2,3], and further extended by the Von Karman Institute by Zimmer et al. [4] or Hald and Buchlin [5]. The modeling of such a problem generally involves a configuration, in which a mixture of water droplets and wet air flowing downward (featuring the spray), is submitted to a strong irradiation from a high temperature source. Various problems have been identified in relation to the dynamics of such two-phase flows. On the other hand, the behavior of an equivalent participating medium has been also considered. Both problems have been addressed separately, but few attempts have been reported on studies combining these difficulties with accurate simulation tools addressing each of them.

For example, the radiative transfer problem has been treated as 1D with azimuthal symmetry, considering that the dynamics is set once for all and the actual spray behaves like an homogeneous equivalent medium with known properties [3]. As a complementary example, care has been brought to the simulation of the flow dynamics [4], uncombined with heat transfer however. When coupling with heat transfer has been addressed, this has been done in [1] with a pseudo 1D model for the dy-

* Corresponding author. Tel. and fax: +3 (33) 383 684 686.
E-mail address: pascal.boulet@lemta.uhp-nancy.fr (P. Boulet).

1290-0729/$ – see front matter
doi:10.1016/j.ijthermalsci.2006.11.005

Nomenclature

C_D	drag coefficient
d_p	droplet diameter ..... m
f_v	droplet volume fraction ... m^3 of water/m^3 of air
m_p	droplet mass ..... kg
$\dot{m}$	droplet vaporization rate ..... $kg\,s^{-1}$
n	mean number of droplets per unit volume ... m^{-3}
N	number of trajectories or loops
P_λ	scattering phase function
$\dot{Q}$	flow rate ..... $kg\,s^{-1}$
Q_{abs}	part of energy lost by a quantum due to absorption
Q_l	heat transfered into the droplet ..... W
Re_p	particle Reynolds number
S_ϕ	source term
S_σ	distance of interaction based on the scattering coefficient ..... m
T	temperature ..... K
T^*	integral time scale of the fluid seen by the particle ..... s
Tr	transmittance
U, V, W	velocity components ..... $m\,s^{-1}$
$\vec{V}$	velocity vector
x, y, z	spatial coordinates ..... m
X, Y, Z	space directions
Y_f	water vapor fraction ... kg of water/kg of dry air
$\vec{X}_p$	particle position ..... m

Greek symbols

β	extinction coefficient ..... m^{-1}
$\Delta x, \Delta y, \Delta z$	grid size ..... m
Δt	time step ..... s
Γ_ϕ	diffusion coefficient ..... $m^2\,s^{-1}$
κ	absorption coefficient ..... m^{-1}
μ	dynamic viscosity ..... Pa s
φ_n	fluctuating property of the fluid
ψ	random part of the fluctuating property φ_n
σ	scattering coefficient ..... m^{-1}
ρ	density ..... $kg\,m^{-3}$
τ_p	particle relaxation time ..... s
$\tau_{p\theta}$	particle thermal relaxation time ..... s

Subscripts

f	continuous phase property
m	mixture property
p	particle or droplet property
λ, ν	spectral or frequency dependent property
0	injection condition

namics and with a two-flux model for the radiative transfer part.

In a similar manner, present authors [6–8] recently studied numerically and experimentally the propagation of radiation through a spray. However, the simulation of the radiation propagation also started with fixed size and moisture distributions a priori given by experiments and assumed to be constant in the whole domain. The use of predicted data for the dynamics was not yet introduced and numerous assumptions were required, among which the most questionable: homogeneous droplet and vapor distributions and arbitrarily fixed dimensions for the spray.

In a larger frame, recent reviews by Grant et al. [9] and Sacadura [10] present numerous works related to fire safety sciences. Various modeling difficulties are considered and corresponding improvements are reported, some directly related to our concern. A combined approach involving efficient available sub-models could now produce relevant information on the complete behavior of the spray.

The present work was carried out in order to undertake a detailed simulation of the flow dynamics and radiative problems, simply starting with the water pressure of the feeding system inducing a given droplet size, known at a definite position related to the injection point (20 cm below the nozzle in the present study). Our goal is to present a simulation tool allowing the prediction of radiation attenuation through the spray, whatever the position, on the basis of realistic and heterogeneous droplet distributions, in a 3D configuration.

The experimental setup which has been developed and presented in Parent et al. [7] is considered for the problem geometry. A single spray is produced by a nozzle in a room. Air flow is induced by droplets. The incident radiation coming from the exit of a Fourier Transform InfraRed (FTIR) spectrometer is directed toward the spray in a small solid angle and the flux is measured after propagation through the spray.

The key steps of the simulation are:

(1) tracking of droplets injected in wet air, taking into account injection conditions, gravity, drag, vaporization and turbulent dispersion,
(2) description of the air flow mainly induced by drag effects,
(3) radiation propagation through this medium owing to corresponding absorption and scattering properties.

This may be achieved using in a first step an Eulerian–Lagrangian technique to simulate the droplet flow and the gas phase induced flow. Alternative approaches could involve a lower computational cost. Eulerian–Eulerian method and Method of Moments are often cited in what concerns the description of the flow dynamics. Both methods involve less equations. However, they need closure models, for example related to phase interactions. Moreover they do not allow a detailed study of individual droplets, an information which is available here, with the Lagrangian tracking of droplets. The two-phase flow results are then exported toward a specific code dedicated to radiative transfer. Complete coupling through specific terms in the energy balance will not be addressed, since radiative

transfer will be considered apart in the second step. Owing to the laboratory scale of the experiments used for the comparisons, this is not a problem, since radiation absorption will be too weak to affect the spray temperature or the droplet evaporation. As a consequence, the present simulation must be thought as a simplified model, since coupling would probably be influent in a realistic application of high-radiation shielding.

The two above-cited steps have received a strong attention separately and a complete bibliography cannot be presented here on two-phase flows on one hand and radiative transfer through participating media on the second hand. The basics of presently used numerical tools can be found in Oesterlé and Petitjean [11], Moissette et al. [12] and Boulet and Moissette [13] in what concerns the dynamics of the spray. Important contributions to the Eulerian–Lagrangian description of spray induced flows may be also found in Rüger et al. [14] or Kohnen et al. [15], among others. In addition, the specific problem of droplet vaporization has received much attention and the work by Abramzon and Sirignano [16] is often presented as a reference. All these studies have been used here.

For the radiative part, Dembélé et al. [2], Berour et al. [17] and Collin et al. [6] have all used the DOM (Discrete Ordinates Method) to solve the Radiative Transfer Equation (RTE). One peculiar difficulty of the problem lies in the highly forward scattering behavior of the medium. Whatever the accuracy of the phase function prediction (for example obtained on the basis of the Mie theory), the angular discretization requires the use of a renormalization of the discretized phase function when applying the DOM technique. It induces a deformation of the scattering distribution whatever the care brought to the modeling. Another particularity of the present study is the 3D treatment, which complicates the solution and increases the computational time, since a very fine angular quadrature is required to deal with this scattering anisotropy. Indeed, the forward scattering is so predominant that specific methods like the Delta-Eddington approximation could be considered as a good candidate for the radiative transfer problem. However, a recent study (involving some of the present authors) on pure radiative transfer through a purely anisotropically scattering medium has indicated that the achieved accuracy cannot be as good with such method as with a Monte Carlo reference solution [18]. The FVM offers the advantage to be conservative, but although requires angular and spatial discretization and therefore also suffers from potential ray effects and numerical diffusion (like the DOM does). These considerations led us to the choice of a Monte Carlo method to deal with the radiative transfer, rather than a DOM technique or even the Finite Volume Method (FVM). Note that the radiation incidence corresponds to a collimated beam at this laboratory stage and computational cost is not expected to be too excessive. Our goal here is to build a numerical code able to deal with the various identified physical phenomena. Numerical optimization is not addressed at this stage. This explains a choice of methods possibly leading to a bigger computational effort and the use of numerous iterations during the numerical solution, as will be seen.

In the followings, the spray dynamics will be first addressed through the description of the Eulerian simulation of the continuous phase, the Lagrangian tracking of the dispersed phase and the numerical processing aimed at the two-way coupling simulation. Then the radiative part of the problem will be dealt with. Complete results will be presented and discussed, the emphasis being put on spectral transmittance computations, in relation with data of the spray dynamics that are directly affecting the result: namely droplet volumetric fraction and size.

2. Dynamics of the spray

Our test case has been defined considering the experimental setup in [7]. The spray is injected in a closed room with dimensions $4 \times 4 \times 4\ \mathrm{m}^3$. The injection is directed downward, from a central position in the room (see Fig. 1). The central planes defined by $x = 2$ m and $y = 2$ m are two symmetry planes when addressing the flow dynamics. Therefore, a quarter of the domain will be considered in the first step of the computation. However, when radiative transfer will be addressed considering an incident beam coming according to the X-direction, only the plane such that $y = 2$ m will be kept as a symmetry plane.

The pressure feed of the nozzle is 1.5 bars, corresponding to a volumetric rate which has been measured to $0.26\ \mathrm{L\,min^{-1}}$. Some data have been fixed following the study by Zimmer [19]. The exit section of the nozzle has an equivalent diameter of 0.53 mm, consequently droplets are injected with an initial velocity around $18.9\ \mathrm{m\,s^{-1}}$. At 20 cm below the injection point, the spray is known to behave as a pulverization with a mean Sauter diameter of 182 μm, a value that will be used for simulations carried out on an expected equivalent monodispersion. When simulating a realistic polydispersion, droplet injection will be considered as to yield the same mean Sauter diameter value at 20 cm, with a 20 class split between 50 and 500 μm. A conic shape has been observed for the spray with ejection angles evaluated as 16° (according to the X-direction) and 40° (according to the Y-direction), yielding an elliptic section perpendicular to the vertical axis.

2.1. Eulerian simulation of the gas phase

Droplet fall induces a turbulent air flow which can be described with balance equations for mass, momentum and energy. Additional equations have to be introduced to deal with turbulence and mass fraction of water vapor in air. The present

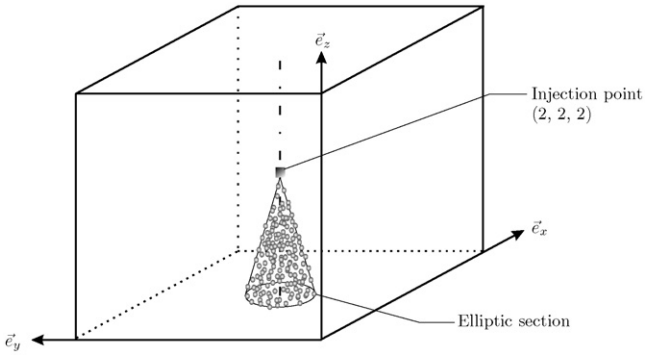

Fig. 1. Sketch of the injection in the room.

work involves a 3D stationary description. The general standard formulation of the corresponding balances may be given as

$$\frac{\partial}{\partial x}\left(\rho_f\langle U_f\rangle\phi\right)+\frac{\partial}{\partial y}\left(\rho_f\langle V_f\rangle\phi\right)+\frac{\partial}{\partial z}\left(\rho_f\langle W_f\rangle\phi\right)$$
$$=\frac{\partial}{\partial x}\left(\Gamma_\phi\frac{\partial\phi}{\partial x}\right)+\frac{\partial}{\partial y}\left(\Gamma_\phi\frac{\partial\phi}{\partial y}\right)+\frac{\partial}{\partial z}\left(\Gamma_\phi\frac{\partial\phi}{\partial z}\right)+S_\phi \qquad (1)$$

where $\langle x\rangle$ denotes the average of the variable x.

In this relation $\phi=1$ leads to the mass balance, $\phi=\langle U_f\rangle$ or $\langle V_f\rangle$ or $\langle W_f\rangle$ yields one of the three momentum equations in the X, Y or Z direction respectively, $\phi=\langle T_f\rangle$ yields the energy balance, $\phi=\langle Y_f\rangle$ the balance for water vapor mass fraction and finally $\phi=k$ or $\phi=\varepsilon$ corresponds to the closure equations aimed at the turbulence modeling.

Γ_ϕ are the corresponding diffusivities adapted to each scalar variable description and S_ϕ corresponds to source terms.

The present Eulerian formulation actually follows a classical modeling. Details for the flow simulation are not repeated here, but can be found in Kohnen et al. [15] or Berlemont et al. [20], among other specific studies related to the continuous phase dynamics. Complementary information specific to the present study is given in the following paragraph.

The source term due to droplets in the momentum equation only comes from drag effects, lift force or other interactions being currently neglected in such problems with relatively high density inclusions as compared to the continuous phase density (see for example Boulet and Moissette [13] for a more complete description). A standard k–ε model is used here for the turbulence closure, for a sake of stability of the whole numerical processing, which can be better warrantied with this well-known robust model. An hybrid formulation of the source terms [13] is introduced in the balance equations for k and ε, with a modeling constant $C_{\varepsilon 3}=1.87$, in order to involve the prediction of turbulence rise due to wake effects behind large droplets. For the heat exchange, the source term is due to vaporization process, as droplets will cool the surrounding air in order to get the required energy to vaporize. Let us recall here, that the experimental device is used at a laboratory scale with a very weak radiative flux coming from a spectrometer. Corresponding radiative source for the flow can be completely omitted in the present application.

2.1.1. Boundary conditions

The setup is located in a room. A cubic enclosure is considered with two symmetry planes as above discussed. Other boundaries are walls. This implies the use of standard wall laws for the dynamics of the flow. Conditions for temperature and water vapor are more difficult to assess. Actually the surrounding air is assumed to be renewed, since the room cannot be considered as hermetically closed. However, inlet and outflow conditions are not simple to introduce and would probably affect the spray dynamics, unless a very huge computational domain is considered. It would induce a penalizing computational cost, aimed at the simulation of areas far from the spray and therefore uninteresting for us. Considering that a stationary picture of the spray is sufficient to provide the droplet distribution, and that the liquid flow rate is too weak to affect the surroundings besides the spray area, Dirichlet's conditions for the walls with constant water mass fraction and continuous phase temperature (typically at 60% of relative moisture and 300 K) have been applied. The temperature had been found to vary very weakly in a former study even when addressing a strong radiative source, due to competing effects between convection, vaporization and radiation [8]. Hence, the present assumption does not rise any sensitivity problem. For the boundary condition devoted to the water vapor fraction, our assumption was found to be more questionable. Therefore tests have been carried out on the sensitivity of our transmittance prediction (detailed in the next section) to the boundary conditions, considering values of 60% and 80% of relative moisture at walls respectively, and investigating the impact on the transmittance computed through the spray. The typical discrepancy has been found to be lower than 0.1% in the case of the typical cases which are discussed below. This test shows that the present assumption does not infer a strong uncertainty in the attenuation prediction.

2.2. Lagrangian tracking of the droplets

The tracking of individual droplets lies in the solution of equations for their position, velocity, temperature and size. Statistics are finally carried out on the basis of each track registered at every time step. Note that hydrodynamic break-up of droplets, possible collisions, and related coalescence effects are not included in the Lagrangian tracking. This is a correct assumption considering the reference paper by Elgobashi [21] and the low volumetric fraction of interest. In this work so-called four-way coupling effects (namely related to particle collisions) are considered to be negligible for volumetric fractions lower than 10^{-3} m^3 of water/m^3 of air, whereas present simulations concern cases with values 10 or 100 times lower. Note also that the injection of individual droplets is considered here, with a definite size distribution equivalent to the observed spray and not the actual liquid film which is supposed to form the droplet phase after break-up processes.

The following set of equations is solved to characterize each followed particle

$$\frac{\mathrm{d}\vec{X}_p}{\mathrm{d}t}=\vec{V}_p \qquad (2)$$

$$m_p\frac{\mathrm{d}\vec{V}_p}{\mathrm{d}t}=C_D\rho_f\pi\frac{d_p^2}{8}\|\vec{V}_f-\vec{V}_p\|(\vec{V}_f-\vec{V}_p)+m_p\left(1-\frac{\rho_f}{\rho_p}\right)\vec{g} \qquad (3)$$

$$m_pCp_p\frac{\mathrm{d}T_p}{\mathrm{d}t}=Q_1 \qquad (4)$$

$$\frac{\mathrm{d}m_p}{\mathrm{d}t}=-\dot{m} \qquad (5)$$

Eq. (3) takes into account drag force and gravity effects. Vaporization influence is taken into account following the suggestion by Abramzon and Sirignano [16]. A correlation by Faeth [22]

is used in order to modify the drag coefficient in relation to the vaporization of the droplet

$$C_D = \frac{24}{Re_p}\left[1 + \frac{Re_p^{2/3}}{6}\right] \tag{6}$$

where $Re_p = \frac{\rho_f V_r d_p}{\mu_m}$ stands for the particle Reynolds number which has to be evaluated with a special care regarding the fluid properties, since ρ_f is the density of the wet air whereas μ_m is the viscosity of the mixture wet air/saturated air, applying the 1/3 rule. $V_r = \|\vec{V}_f - \vec{V}_p\|$ is the relative velocity of the particle.

Eq. (3) yields the temperature evolution addressing the respective influence of convection and evaporation (radiation absorption by droplets is omitted when simulating our spectrometry experiments as above-mentioned). On the basis of the work by Abramzon and Sirignano [16] Q_1 is expressed as

$$Q_1 = \dot{m}\left[\frac{Cp_v(T_f - T_p)}{B_T} - L_v\right] \tag{7}$$

with the vaporization rate

$$\dot{m} = 2\pi d_p Sh^* \rho_m \mathcal{D} \ln[1 + B_M] \tag{8}$$

Cp_v is the heat capacity evaluated for the water vapor. B_M and B_T are the Spalding mass and heat transfer numbers introducing the role of water vapor fraction and temperature gradients. They are computed in a combined process involving Sherwood (Sh^* in the above equation) and Nusselt numbers in modified forms and introducing thermophysical properties computed at a film temperature obtained with the 1/3 rule. In particular ρ_m and $\mathcal{D}$ are average density and binary diffusion coefficient of the gas in the film (see Abramzon and Sirignano [16] for complete details and sensitivity study on the vaporization problem).

In addition to its influence on the heat exchange, evaporation also modifies the droplet size as the droplet is falling. The mass loss is therefore introduced in relation (5) to predict the size decrease, m_p being related to d_p^3.

Whenever the fluid phase plays a role in the above relations through its velocity and temperature, the characteristic which is of interest is the "instantaneous fluid property seen by the particle". That means that data exported after the Eulerian step presented in the previous paragraph cannot be directly used, since they correspond to local mean values of the continuous phase. A fluctuating part has to be added to the average property in order to yield an instantaneous value. These turbulence effects are addressed on the basis of a dispersion model which has been used by Moissette et al. [12]. This is a first order stochastic model, in which each fluctuating property φ_n computed at time $t = n\Delta t$ and position $X_p(t)$ is written as a function of its value at the previous time step and location, introducing a complementary random part

$$\varphi_n = \varphi_{n-1} \exp(-\Delta t / T^*) + \psi_n \tag{9}$$

where T^* stands for an integral time of the fluid seen by the particle and ψ_n is a Gaussian random variable with zero mean value. Every variable φ has its own random part ψ. They are determined so as to fulfill conditions required by the Reynolds stress tensor and the turbulent heat fluxes yielded by the Eulerian simulation of the continuous phase (computed using a Simple Eddy Diffusivity (SED) model). A description dedicated to the complete determination of the ψ and T^* data may be found in [12].

The numerical processing involves the tracking of a large number of droplets. The time step of the tracking is computed as

$$\Delta t = \min\left\{\frac{\tau_p}{10}, \frac{\tau_{p\theta}}{10}, \frac{1}{10}\frac{\Delta z_0}{V_{p_0}}\right\} \tag{10}$$

where

$$\tau_p = \frac{4}{3}\frac{\rho_p}{\mu_f}\frac{d_p^2}{C_D Re_p} \quad \text{and} \quad \tau_{p\theta} = \frac{\rho_p Cp_p d_p^2}{6 Nu_p \lambda_f} \tag{11}$$

τ_p is a classical form of the particle relaxation time based on the dynamics, $\tau_{p\theta}$ is a similar time characterizing the heat exchange by convection around the droplet (with Nu_p the particle Nusselt number and λ_f the fluid phase thermal conductivity) and $\frac{\Delta z_0}{V_{p_0}}$ is the minimum time required to cross a cell vertically for a droplet (Δz_0 being the size of the smallest cell in the grid and V_{p_0} the injection velocity of the droplet and so its maximum value).

Direct integration of the equations has been applied, considering constant properties for the droplets during one time step and explicitly writing solutions for Eqs. (2)–(5) as first order differential equations in time.

Actual liquid flow rate has to be controlled and calibration of dispersed phase statistics is performed balancing the real water amount and the computed value after each tracking process. All the tracks left by each droplet are registered for the statistics and are all taken into account to yield the following numerical flow rate

$$\dot{Q}_{\text{num}} = \sum_{i=1}^{N_{\text{tot}}} \frac{1}{\Delta t_{\text{tot}}} \sum_{j=1}^{n_i} \pi \frac{d_{pi_0}^3}{6} \tag{12}$$

where Δt_{tot} is the total tracking time, N_{tot} is the total number of computed trajectories, n_i is the total number of registered tracks for the ith droplet and d_{pi_0} is the initial diameter of the ith droplet (the injected flow rate has to be sought ignoring any change in the liquid amount due to evaporation).

Every data are then corrected multiplying by the ratio of the real rate over the numerical value: $\dot{Q}_{\text{real}}/\dot{Q}_{\text{num}}$.

Droplets are followed till they reach the bottom of the computational domain, then they are considered as escaped (rebound influence is not considered).

2.3. Numerical handling—Two-way coupling for the dynamics

The Finite Volume Method with the SIMPLE algorithm is used for the solution of the Eulerian description of the induced air flow. A classical scheme with staggered grids is applied, as described for example in Versteeg and Malalasekera [23].

Source terms in the continuous phase formulation on one hand, or fluid velocity and temperature use in the droplet tracking on the other hand, induce the respective influence of one phase on the other. Corresponding effects can be numerically

taken into account using an iterative method in order to obtain a solution for the whole problem.

A first stage of convergence is sought on the dynamics solely. Then, heat transfer and vaporization effects are taken into account. The complete numerical handling involves the following steps:

(1) first tracking of N_d droplets in air at rest, discarding evaporation, heat transfer and turbulent dispersion in the trajectory computation in order to minimize the computational time of this early stage of the calculation, registering each track and computing its contribution to the various source terms aimed at the modeling of the dispersed phase influence on the continuous one.
(2) Solution of the Eulerian simulation for the air flow in isothermal condition, taking into account the previous step results for the dispersed phase that will induce the air flow due to drag effects.
(3) Tracking of N_d droplets in the corresponding flow field without heat transfer and vaporization, evaluating corrected source terms to be introduced in the next Eulerian solution step.
(4) Solution for the Eulerian simulation of the fluid phase in isothermal conditions taking into account the corrected statistics yielded by the previous step, performing N_E iterations.
(5) Repetition of steps (3) and (4) until convergence is appraised to be sufficient, the number of iterations warranting that the so-called two-way coupling effects have been correctly taken into account.
(6) Repetition of steps (3) and (4) activating vaporization effects and heat transfer, until complete convergence is reached.

Typically, N_d is of the order of 150 000 droplets. Considering that each droplet may leave more than 1000 tracks which are all registered, the statistics are performed on a really large number of tracks. In what concerns the Eulerian part of the computation, N_E is typically equal to 200. Finally, in order to take into account the two-way coupling effects, repetition of steps (3) and (4) can be as large as 100. Of course optimization of the whole process could be sought, regarding the computational cost in particular. This was not considered as a priority for the moment.

If a polydispersion is considered, computations are first carried out on monosize droplets with diameter equal to an evaluated mean Sauter diameter. After a first simulation following the above detailed step, computations are completed on the actual polydispersion through repetition of steps (3) and (4), starting with the initial values obtained on the monodispersion.

The typical mesh is presented on Fig. 2. The grid size in the present case is $24 \times 24 \times 40$. This is a structured mesh which has been defined following a specific preliminary study in order to check that numerical predictions are grid independent [24]. In particular the mesh has been set involving: (i) smaller cells near the walls, checking the required criterion for the use of the so-called wall laws (usual distance between the wall and the first cell center larger than 30, in wall units); (ii) smaller cells near the spray injection position, with a size affecting the Lagrangian time step used for the tracking, warrantying that droplets are leaving several tracks in each traveled cell (optimal parameters chosen after an analysis of the statistical results provided by the droplet tracking); (iii) a good compromise between time cost and accuracy (preliminary tests with grids involving various mesh size have qualified the present $24 \times 24 \times 40$ grid as the best compromise). Regarding the central area, where the spray is injected, 8 thin regular cells are concentrated just before location $x = 2$ m and just below location $y = 2$ m. This refinement makes easier the numerical simulation in this area where the gradients and the coupling terms are large. This also allows to export accurate evolutions of the droplet size and volumetric fractions (of droplets and vapor), to be used in the simulation of the radiation propagation.

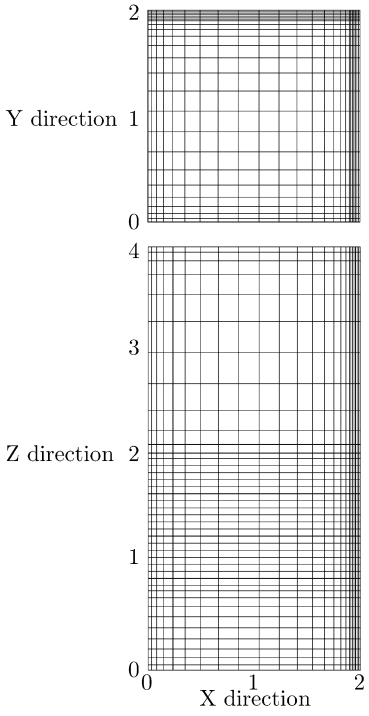

Fig. 2. Visualization of the grid in central planes (XY and XZ orientations).

Note that convergence is not easy to assess, owing to the fact that a check for residuals (for example defined for each variable as a sum on every nodes of the relative discrepancy between two successive iterations) as it is often done in the case of one-phase flows cannot be simply used. This has been discussed by Kohnen et al. [15]. Indeed each injection induces a fluctuation in the source terms around an average value. When a sufficient number of Eulerian–Lagrangian couplings has been addressed, this does not really affect the mean characteristics of the flow, but it disturbs the residuals however, with a similar jump after each Lagrangian step followed by the same decrease during the Eulerian step. Instead of restricting our convergence verification to such residuals (which are of course also computed), the evolution of sensitive variables is studied as more reliable convergence criteria iteration after iteration (as it was suggested by Kohnen et al. [15]).

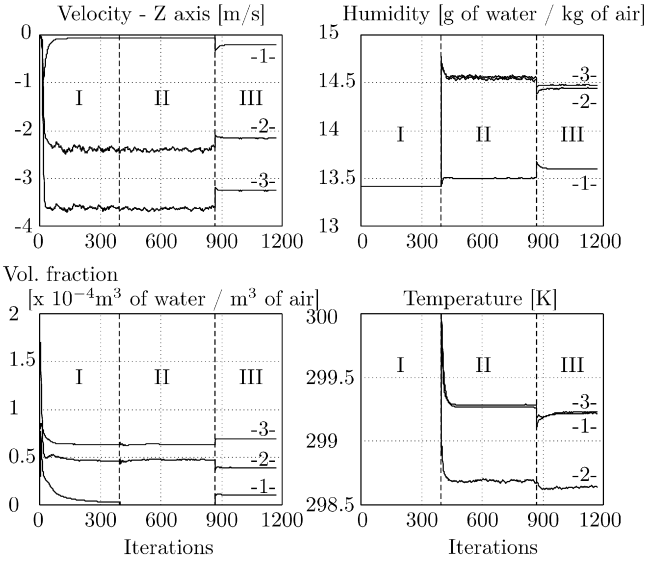

Fig. 3. Key variable evolution during the iterative calculations. Label -1-: position ($x = 1.92$ m, $y = 2$ m, $z = 1.10$ m). Label -2-: position ($x = 2$ m, $y = 2$ m, $z = 1.10$ m). Label -3-: (position $x = 2$ m, $y = 2$ m, $z = 1.76$ m). Area I monodispersion without heat transfer and evaporation. Area II monodispersion under complete simulation. Area III polydispersion under complete simulation.

Results are presented on Fig. 3 where the driven air flow velocity, the water vapor mass fraction in air, the air temperature and the droplet volumetric fraction have been plotted after each complete Eulerian–Lagrangian loop for three positions (two points below the injection point and one point shifted from the injection axis). Curves noted -1-, -2- and -3- give the results for these three points with respective coordinates ($x = 1.92$ m, $y = 2$ m, $z = 1.10$ m), ($x = 2$ m, $y = 2$ m, $z = 1.10$ m) and ($x = 2$ m, $y = 2$ m, $z = 1.76$ m). In particular, vapor mass fraction and droplet volumetric fractions are input data for which the convergence has to be checked, since they are required for the radiative part of the problem, as will be discussed in the section dedicated to radiative transfer. Numerical conditions correspond to those studied in the next paragraphs. As can be seen, the number of coupling loops (repetition of above cited steps (3) and (4)) is very large in the present test case devoted to the observation of the computational stability. About 400 Eulerian–Lagrangian loops have been first carried out, injecting monosize droplets without evaporation and heat transfer (explaining why the curves for humidity and temperature do not vary during this first stage, in the area labeled I). All variables have reached a stable value, before the end of the step. Then 400 further iterations have been performed for the complete heat and mass transfer problem still considering monosize droplets (area labeled II). Water vapor mass fraction and temperature are of course sharply varying at the beginning of the step, but they reach a converged value quickly. The other characteristics are not affected by the introduction of heat transfer and evaporation phenomena (knowing that the liquid flow rate and the energy exchange are weak in the present study). Finally, area III corresponds to the complete simulation performed on the actual polydispersion, starting with the initialization yielded by the monodispersion characterized along area II. One can see that after a quick correction of the previous monodispersed data, the convergence of all variables is reached and all tracers are stable.

Of course the number of loops can be obviously roughly reduced if an optimal solution regarding this feature is sought, stopping the computations earlier.

2.4. Results for the spray dynamics exported for the radiative transfer study

The case of the spray depicted at the beginning of this section is presented. Based on reference data [19], the polydispersion is injected considering a Rosin–Rammler law and involving 20 classes between 50 μm and 500 μm, with a Rosin–Rammler mean diameter at the injection point of 310 μm and a dispersion parameter of 2.66. At 20 cm below the injection point, the computed mean Sauter diameter is 180 μm (in accordance with the measured value of 182 μm). In the present paragraph results will be also compared with those obtained simulating a monodispersion of droplets (diameter equal to 182 μm) for the same flow rate (0.26 L min^{-1}). We are especially interested in the results useful for the radiation attenuation study, namely the droplet volumetric fraction and size as a function of the position in the spray.

Fig. 4 is a representation of the spray through the tracks left by two opposite classes of droplets along their fall during a typical Lagrangian step. Left-hand side figure presents typical behavior of droplets with size around 465 μm, right-hand side figure is for 85 μm particles. These representations have been taken from the same complete polydispersion simulation. The shape of the spray illustrates the zones usually observed experimentally: a conic shape especially near the top and trajectories closer to a vertical fall below. Large droplet trajectories keep directions affected by their injection angles all along their fall, whereas small droplet trajectories are quickly governed by the vertical driven air flow. Globally, large droplets are creating a core which is filled by small droplets, leading to a droplet distribution which is obviously heterogeneous. As expected, large droplet trajectories are also close to lines since they are little affected by turbulent dispersion, whereas the tracks left by small droplets yield more fluctuating trajectories.

The heterogeneity in the droplet distribution can be also illustrated, computing the evolution of the mean Sauter diameter (labeled D_{32}) as a function of the vertical position. For each z position, an integration has been performed on a XY plane to yield the mean size of droplets. Fig. 5 presents the obtained results in comparison with the near constant value also computed for the monodispersed case. Indeed a weak decrease in the monodispersion value is obtained as a consequence of evaporation, that results in a size decrease. As can be seen this size loss is very weak, droplets are falling too fast to be really affected by evaporation regarding their size (this is in accordance with the remark of the previous section, on the weak sensitivity of results with respect to evaporation phenomena in the present problem). The evolution in the polydispersion case is more complex. A first decrease is observed with a minimum value reached near 170 μm, followed by an increase till a near constant value is reached more than 1 m below the injection.

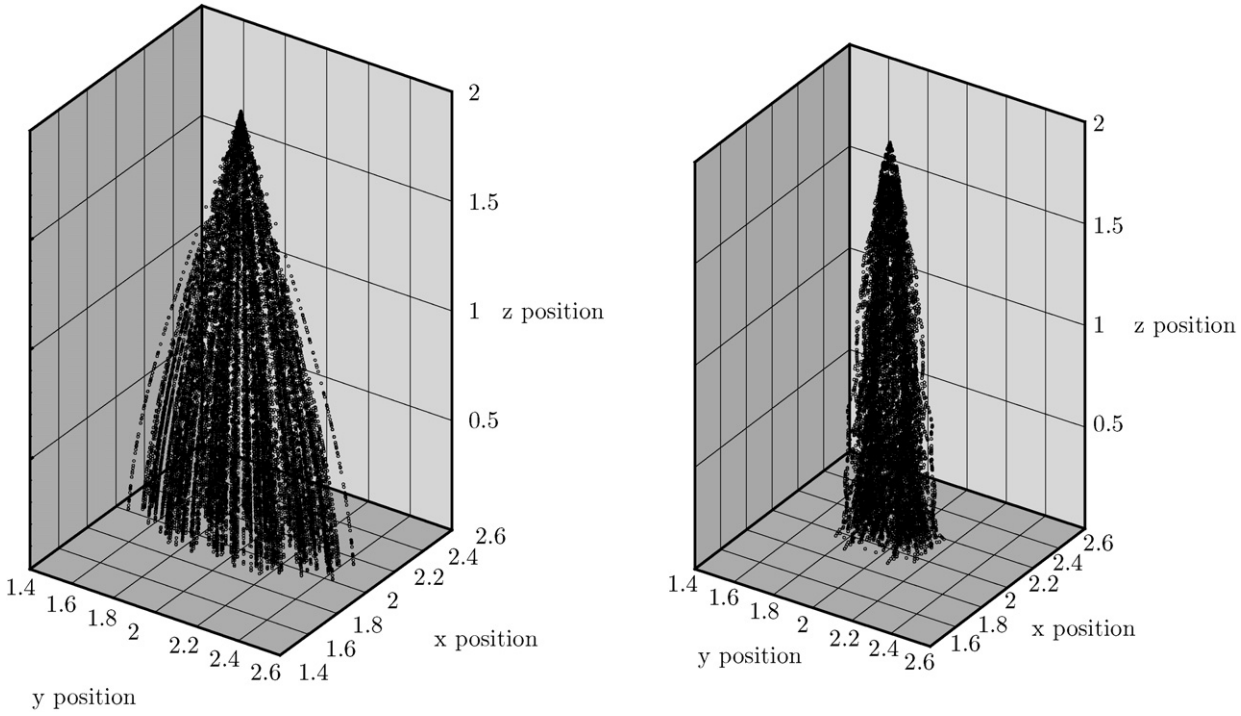

Fig. 4. Typical droplet distribution in the spray. Each point is a track left by a droplet during a post-processing computation. Left-hand side: 465 μm droplets. Right-hand side: 85 μm droplets.

The discrepancy in the droplet behaviors as a function of their relative size can explain this result on D_{32}. Near the injection area, on the top, large droplets still fall with a high velocity, contributing in a weak manner to the averaged size, whereas small droplets are already slowed down, they leave numerous tracks in cells and bring a large weight to the computation of the mean size. As the vertical position decreases the velocity of each droplet class decreases and reaches its limit value. Each class contributes more and more to the computation of the average size, leading to an increase of D_{32} until a diameter close to 210 μm is obtained (the second step of size decrease is probably induced by the flow near the floor more than by evaporation effects, but our study is not carried out in order to yield a specific description of this area).

Fig. 6 presents the volumetric fraction of droplets on a central plane ($y = 2$ m) at different vertical position under the spray injection, along an horizontal line parallel to the X axis, the main radiation propagation direction. The right-hand side figure is for the polydispersion. The spray width is seen to increase with the distance from the injection, and the water volumetric fraction is maximum at the spray center. On the left-hand side figure, corresponding results are given for the monodispersion. An amazing result is obtained, since droplets apparently shift from the spray center. Indeed, the tracking is performed on relatively massive particles and their trajectory is first governed by the injection angle that shifts them away from the injection line. Then, drag and gravity effects pull them vertically and they are little affected by horizontal motion (which could be due to dispersion effects for example). When considering a polydispersion, large classes present a similar behavior, but small droplets are entrained in the core region and the overall

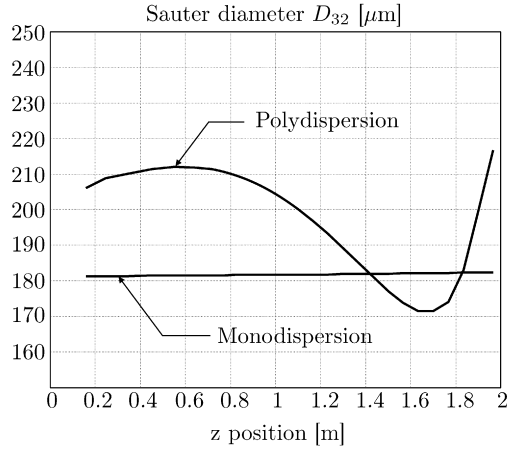

Fig. 5. Mean Sauter diameter averaged on the XY plane as a function of vertical position.

volumetric fraction does no more exhibit an empty spray core. Note that computations have been also performed on the cumulative volumetric fraction along the X direction for the different curves (not shown here, but corresponding to the integral of the curves presented on Fig. 6). It yields the total quantity of water integrated along a line similar to the direction of radiation propagation for various vertical positions. Results obtained for the monodispersion indicate a strong increase when moving away vertically from the injection position. This can be explained by a decrease in the droplet velocity due to drag effects, leading to an increase in the global volumetric fraction. On the contrary, the increase is relatively small for the polydispersion. In this case small droplets are slowed to their terminal velocity before

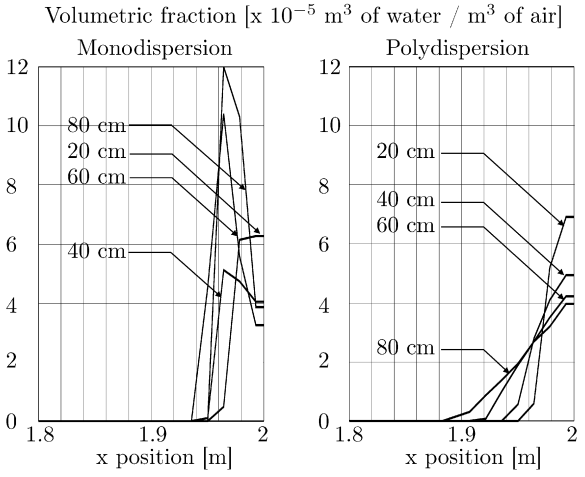

Fig. 6. Volumetric fraction of droplets along the X axis at 20, 40, 60 and 80 cm below the injection point. Case of a monodispersion of 182 μm droplets (left figure) and a polydispersion (right figure).

they reach the 20 cm position and their contribution to the volumetric fraction remains constant. Large droplets behave like those of the monodispersion but their influence is hidden and the increase for the global water amount with the vertical position in the pulverization is weak.

What is obvious in the above comments is the discrepancy in the prediction when addressing a monodispersion or a polydispersion. In the next section, computations will be carried out on radiation propagation on the basis of these data, in order to investigate the consequences of these differences.

3. Radiative transfer through the spray

Our problem is the computation of transmission of infrared radiation through the spray. In a classical manner, this absorbing and scattering medium has to be characterized through its radiative properties: absorption and scattering coefficients complemented by the scattering phase function. One important and well-known feature is the strong dependence of these radiative properties with the wavelength. A special care has to be devoted to this peculiarity. Note that emission by the medium itself has not to be taken into account, since the experiments used for the validation have been performed using a Fourier Transform InfraRed (FTIR) spectrometer. The radiation emitted by the spray itself is not coherent with the incoming radiation yielded by the source and does not contribute to the interference pattern analyzed by the spectrometer. The next subsections give details on the radiative property computation and on the radiation propagation simulation.

3.1. Radiative properties

Once the dynamics of the flow has been predicted, values for the droplet distribution and the vapor mass fraction are known in every cells of the mesh. They will provide input data for the computation of local radiative properties of the equivalent medium made of droplets and gas, through which the radiation will propagate. Owing to the low volume fractions of interest (maximum local value around 10^{-4} m^3 of water/m^3 of air), a simple addition of the radiative properties can be considered, in particular assuming that independent scattering prevails in the present problem. Consequently the absorption coefficient of the global medium is a simple sum of the droplet and gas contributions, whereas scattering properties are solely due to droplets:

$$\kappa_\lambda = \kappa_{\lambda_p} + \kappa_{\lambda_f}$$
$$\sigma_\lambda = \sigma_{\lambda_p}$$
$$P_\lambda(\vec{\Omega}' \to \vec{\Omega}) = P_{\lambda_p}(\vec{\Omega}' \to \vec{\Omega}) \tag{13}$$

The Mie theory yields the radiative properties of the droplets. Water optical index is taken from Hale and Querry study [25]. The reader is referred to recent contributions in Berour et al. [17] and Collin et al. [6] for a recall of the detailed formulation and a sensitivity analysis on the radiative properties. In particular the role of the droplet size has been discussed, recalling the stronger ability of small droplets to absorb and to scatter radiation in comparison with large droplets, if the same water content is considered.

The gas phase induces the difficulty of dealing with extremely sharp spectral variations. The gaseous species of interest, regarding possible interactions with radiation, are mainly water vapor and possibly carbon dioxide. Following the work by Soufiani and Taine [26] a C–K model provides a very good compromise between the expected accuracy for characterizing these gases and computational time, especially with the 43 band model considered here (see [26] or [6] for a complete description of C–K model implementation).

The acute anisotropic scattering is another well-known characteristic of water sprays. Typical phase function shapes for water droplets in the size range of the present study have been plotted in Berour et al. [17] and are not reproduced here. To illustrate the importance of the peak in the forward direction, let us just recall that for a wavelength of 2.5 μm (around the maximum emission for typical sources in our fire safety related problems) and the mean droplet diameter 182 μm, the size parameter is 229 (larger values are of course even obtained for the largest droplet classes). Hence, the asymmetry factor for the phase function in this case reaches a value as large as 0.93. As discussed in the introduction, a way to avoid the problem related to anisotropic scattering, is to simulate the radiation propagation with a Monte Carlo technique (no angular discretization involving a renormalization process is required). Moreover, as will be seen hereafter, the phase function will be handled with, on the basis of its cumulative function, which suppresses the problem of sharp variations since the increase with the cosine of the scattering angle is monotonic.

The originality of the present results lies in the possibility to observe the spatial evolution of the radiative properties, instead of simply considering an equivalent homogeneous medium with constant averaged properties. To illustrate this point, Fig. 7 presents the optical thickness computed on the basis of the spectral extinction coefficient ($\beta = \kappa + \sigma$), evaluated at the wavelength 1.1 μm, as a function of the x position, on two lines parallel to the X direction. They are respectively defined 80 cm under the injection point ($y = 2$ m, $z = 1.2$ m) and

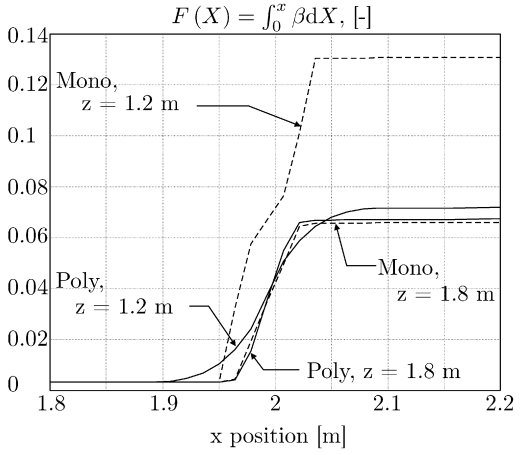

Fig. 7. Optical thickness along the X direction for two lines parallel to the main direction of radiation propagation, defined by ($y = 2$ m, $z = 1.2$ m) and ($y = 2$ m, $z = 1.8$ m). Wavelength: 1.1 μm.

20 cm under the injection point ($y = 2$ m, $z = 1.8$ m). A zoom is plotted in the spray area (1.8 m $< x <$ 2.2 m), since the increase of the presented variable is observed where droplets are numerous. As a result, optical thickness raises along the path followed by the radiation crossing the spray, from the spectrometer, toward the detector. This wavelength is the only one discussed here, since the same trends have been observed whatever the wavelength in the range [1 μm, 10 μm]. Computations have been carried out for the polydispersion and the monodispersion. When considering the polydispersion, one can see that the overall optical thickness reaches similar value (a little larger for the position 1.2 m), leading to the assumption of equivalent attenuation ability for the spray when varying the vertical position below the injection point (at least for these two positions). Nevertheless, the increase in the optical thickness is effective on a larger range of x position, as a consequence of a larger spray section when increasing the distance from the injection. Note also the non-linear increase, which indicates the heterogeneity of the radiative properties in the spray.

When considering the monodispersed spray (with 182 μm droplets), results are of course in accordance with the polydispersion at the position where the mean Sauter diameter is close to 182 μm (at $z = 1.8$ m). However, as the D_{32} has been observed to vary with the vertical position when addressing the actual polydispersion (Fig. 5), the monodispersion prediction at $z = 1.2$ m is obviously far from the actual polydispersion prediction. For the monosize spray, the diameter remains quite constant (beside weak evaporation effects) but the volumetric fraction has been found to increase (see Fig. 6), leading to an increase in the optical thickness. On the contrary for the polydispersion, the mean size is larger at $z = 1.2$ m (see Fig. 5) and a weaker attenuation ability could therefore be expected according to the Mie theory. As the optical thickness is observed to vary very slowly, one can conclude that competing effects due to the volumetric fraction are involved (a slight increase as above discussed) in order to keep a near constant attenuation whatever the vertical position in the spray.

3.2. Monte Carlo technique

The radiative properties of the equivalent medium being known as a function of spatial location and wavelength, the radiation propagation may be simulated. A complete review of the Monte Carlo techniques may be found in Modest [27] and Wong and Mengüc [28], among others. A large number of quanta are tracked in the medium, computing scattering and absorption events undergone by the radiation on the basis of probability functions that fulfill the actual radiative properties of the medium. A post-processing step is performed consisting in a statistical treatment of the tracks left by every quanta and yielding the required information: exchanged radiative fluxes or, in the present case, transmission characteristics of the medium.

The so-called MCM2 technique suggests the computation of a distance of interaction on the basis of the scattering coefficient. Other possibilities lie on the absorption or the extinction coefficient (see [28] for a complete description). The MCM2 method in a slightly modified form has been chosen here, after a sensitivity analysis providing an optimal behavior of the method and leading to a compromise between computational time and accuracy. The distance of interaction S_σ evaluated along the quantum path is defined as

$$R_\sigma = \exp\left(-\int_0^{S_\sigma} \sigma \, \mathrm{d}s\right) \tag{14}$$

introducing a random number R_σ with uniform density probability between 0 and 1.

Along the distance S_σ, the part of the energy lost by the quantum due to absorption is

$$Q_{\mathrm{abs}} = 1 - \exp\left(-\int_0^{S_\sigma} \kappa \, \mathrm{d}s\right) \tag{15}$$

The complementary part, $1 - Q_{\mathrm{abs}}$ is consequently scattered at the end of the distance of interaction. A random choice based on the actual scattering phase function used in a cumulative form is performed to determine the new direction of propagation for the quantum before a new interaction event.

The modification of the MCM2 method (the present evolution could be considered as a MCM2.1 method) is related to the fact that the non-scattered part is not totally absorbed by the medium at the position reached after the distance S_σ. Instead, the trajectory of the quantum through the successive cells is built and the absorption is split into successive absorbed parts, providing to each cell the fraction of the energy that it has taken to the quantum as a function of the corresponding run path. In addition to an accurate description of a progressive energy absorption, this allows to take into account the local variations of the absorption coefficient when entering in different cells, since radiative properties are varying as a consequence of the predicted spray dynamics.

The present Monte Carlo technique has been tested in order to yield converged results unaffected by the choice of the number of tracked quanta. Tests have been carried out for an increasing number of quanta, in the same numerical conditions

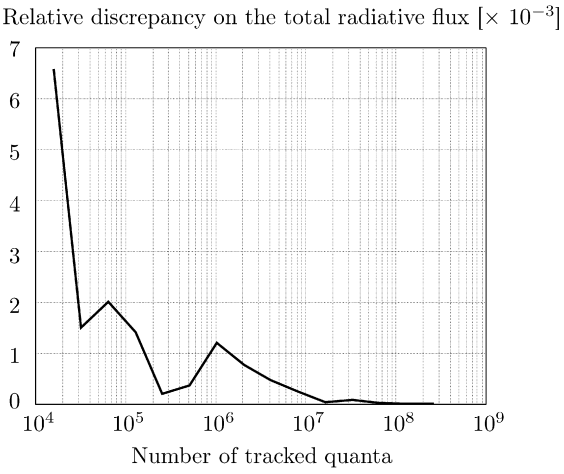

Fig. 8. Sensitivity test on the present Monte Carlo technique. Numerical conditions of Fig. 9. Relative discrepancy is computed comparing a given run and the previous one, which considers a tracking with a half number of quanta.

.

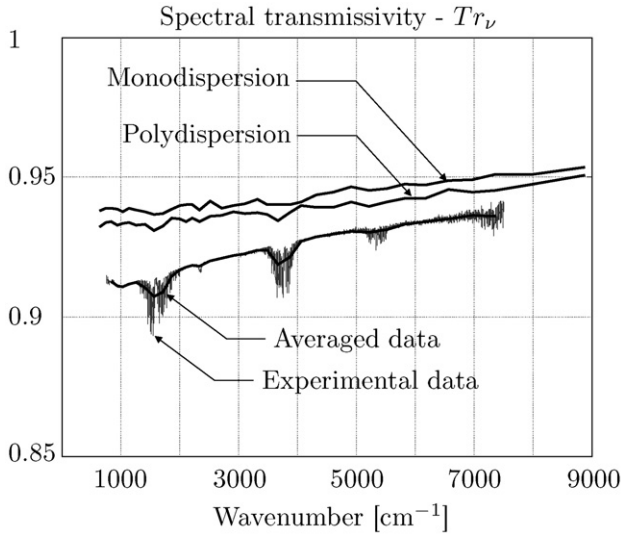

Fig. 9. Spectral transmittance through the spray. Grey curve is for the experimental data with a 2 cm^{-1} resolution, superimposed continuous curve is the result of averaging these experiments on bands corresponding to the 43 band model, other continuous curves are for numerical results. All results are for vertical position 20 cm below injection.

as in the result section. Computations have been started when the collimated beam is simulated tracking 16 000 quanta. Then successive runs have been performed doubling this quantum number, each time. The total flux has been calculated at the detection position and relative error between two successive runs has been computed. Results are plotted on Fig. 8. The discrepancy quickly reaches very small values. Based on this test, radiative transfer simulation presented in the result section have been carried out tracking 2×10^8 quanta, warrantying the quality of the statistical results.

3.3. Results

The spray which has been characterized in Section 2 in what concerns the flow dynamics is used here, with radiation crossing the pulverization along the smallest axis of the elliptic section (X direction). What is called "transmittance" here, is computed as it has been measured with the ratio

$$Tr_\nu = \frac{\text{transmission acquisition with the spray on}}{\text{transmission acquisition with the spray off}} \tag{16}$$

As can be seen, this is not a "true transmittance", featuring the ratio between fluxes entering and leaving the medium, but it yields an information on the ability of the medium to weaken a given incident radiation.

The collimated incident beam is produced in a solid angle of 3×10^{-5} sr. The detection is performed on an area of 4.5×4.5 cm^2 (corresponding to the surface of the spherical mirror collecting the leaving radiation in order to focus it toward the detector), in a solid angle around 8.7×10^{-6} sr.

Measurements have been carried out with a 2 cm^{-1} spectral resolution. Complete description of the experimental setup and acquisition process may be found in [7]. In order to allow a comparison with the present simulation results, experimental data have been also averaged on wavelength bands corresponding to the 43-band model used here.

Fig. 9 presents the comparison between experimental and numerical results 20 cm below the injection point on a central line in the spray ($y = 2$ m, $z = 1.8$ m). Of course experimental data exhibits finer spectral variations, but spectral evolution is in good agreement when comparing data rebuilt with the same spectral resolution than the numerical one (thick curve). Note that the influence of the gases is slightly underestimated numerically. The transmittance level is little overestimated but its increase as the wavenumber rises is well captured. Finally, one can see that the prediction carried out on a monodispersed spray with an equivalent size leads to a satisfactory prediction, since a correct estimation of the mean Sauter diameter is available here. The discrepancy between numerical and experimental data (around 1.3% on the total transmittance) is not surprising considering the double uncertainty on the transmittance measurement on one hand (reasonably estimated around 1%) and on the granulometric information introduced in the simulation on the other hand (data already used by present authors, measured in a previous study [19], on the same type of nozzle but with unknown uncertainty). Supplementary approximation can affect the liquid flow rate and the exact surrounding air humidity. Indeed, an error in the droplet size distribution or in the liquid flow rate may produce an uncertainty in the radiative results, since radiative properties will be affected. Such problems have been studied and quantified in [24], where tests computed in conditions similar to the present result section are presented. As an example, when varying the mean droplet size in the range ±5%, transmissivity has been affected by a discrepancy around 1%. When varying the liquid flow rate in the same range ±5%, transmissivity has been affected by a discrepancy around 0.5%.

Such comparison was previously presented with a simplified numerical approach, showing a correct agreement in this particular case (also presented in [7]). However, the numerical prediction was based on a series of assumptions, involving constant radiative properties and fixed medium thickness. The

problem was the difficulty to extrapolate those data (obtained through local observations and numerical optimization) to another position in the spray. With the present approach that first predicts the spray dynamics whatever the position in the spray, before exporting the required data toward the radiative part of the problem, simulations can be now carried out at any other positions in the water curtain. This will be done in the next paragraph and comparisons will be still performed with the same monodispersion, demonstrating that simplified data in a correct agreement with the measurements at a given location, may lead to inaccurate predictions down in the spray.

Our previous experimental investigation [7] had also indicated that the transmittance was quite the same at different vertical position in the spray. Actually the measured transmittance integrated over the whole wavelength range had yielded the following results: 92.5% at 20 cm below the injection point, 93.0% at 40 cm and 92.1% at 60 cm (respective curves as a function of wavelength would be quite superimposed).

Corresponding computations have been carried out on the previous polydispersion and monodispersion at 20, 40, 60 and 80 cm below the injection point (Fig. 10). As can be seen for the polydispersion, despite changes in the mean size (observed on Fig. 5) and in the spatial droplet volumetric fraction (observed on Fig. 6), competing effects finally yield a near constant attenuation ability with the vertical position, as observed experimentally. On the contrary the monodispersion assumption lead to a decrease in the transmittance (that means a potential overestimation of the attenuation ability) in conjunction with a predicted increase of the optical thickness, as above discussed.

Note that the present apparent conclusion of a constant attenuation as a function of vertical position only holds for a collimated irradiation and a direct transmittance evaluation, in the particular conditions of a laboratory single spray. Modification of the setup could perhaps infer a varying attenuation, especially when considering the case of a real water curtain used for fire radiation shielding.

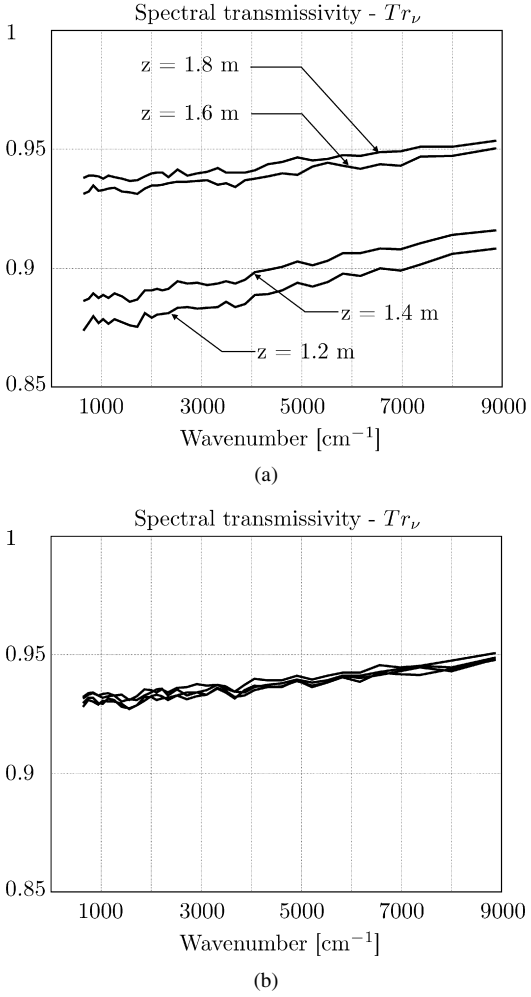

Fig. 10. Spectral transmittance prediction at various vertical position: 20, 40, 60, 80 cm below the injection point. (a) Monodispersion simulation. (b) Polydispersion simulation (curves quite superimposed).

4. Concluding remarks

A fine simulation has been presented on a single spray, from dynamics to radiative transfer. An Eulerian–Lagrangian simulation of the flow has been first carried out and data have been exported in a Monte Carlo simulation for the radiation propagation through the spray. Results have been produced on all characteristics of the medium, including the volumetric fractions, the spatial evolution of the droplet size and finally the transmittance. The feasibility of such a complete simulation has been demonstrated in a 3D configuration. One advantage of the present approach is the possibility to compute heterogeneities in the spray and to produce a real 3D analysis. This results in the computation of the spatially varying radiative properties and do not require the hypothesis of equivalent average properties, assumed constant everywhere in the spray.

Direct spectral transmittance through the spray under collimated irradiation has been simulated and compared with experimental data taken from a previous study. The comparison is satisfactory since the discrepancy is in the uncertainty range of the involved measurements.

In the present case of a single spray with a low flow rate the attenuation has been found constant for various vertical positions in the spray between 20 and 80 cm below the injection point (numerical predictions confirmed by the experimental results).

Computations carried out on an equivalent monodispersion have been found in accordance with the actual polydispersion simulation only at the location where the mean droplet size corresponds to the diameter entered for the monosize spray. Along the vertical position, the droplet distribution and their size are indeed varying in a complex manner, that cannot be captured through a monodispersed simulation.

The predicted radiation attenuation is in good agreement with the experimental data used for the comparison at the present laboratory scale. Further tests will concern more realistic conditions related to radiation shielding at a larger scale (diffuse and stronger incident radiative flux combined with larger water flow rates).

Acknowledgements

Authors thank Professor Oesterlé of the LEMTA for his help and advice, concerning the part of the problem devoted to the simulation of the flow dynamics, based on an Eulerian–Lagrangian technique.

References

[1] H. Prétrel, J.M. Buchlin, Theoretical study of radiative shield with liquid sprays, in: Proceedings of 2nd European Thermal Sciences and 14th Nat. Heat Transfer, Roma, 1996, pp. 937–944.
[2] S. Dembélé, A. Delmas, J.F. Sacadura, A method for modeling the mitigation of hazardous fire thermal radiation by water spray curtains, ASME J. Heat Transfer 119 (1997) 746–753.
[3] S. Dembélé, J.X. Wen, J.F. Sacadura, Experimental study of water sprays for the attenuation of fire thermal radiation, ASME J. Heat Transfer 123 (2001) 534–543.
[4] L. Zimmer, P. Boulet, J.M. Buchlin, Experimental and numerical study of flat fan sprays under lateral wind, in: Proceedings of the 4th International Conference on Multiphase Flow, New Orleans, USA, 2001, page paper 176.
[5] K. Hald, J.M. Buchlin, Thermal shielding by impinging water spray curtains, in: Proceedings of Eurotherm 73 on Computational Thermal Radiation in Participating Media, Mons, 2003, pp. 379–387.
[6] A. Collin, P. Boulet, D. Lacroix, G. Jeandel, On radiative transfer in water spray curtains using the discrete ordinates method, J. Quant. Spect. Rad. Tran. 92 (2005) 85–110.
[7] G. Parent, P. Boulet, S. Gauthier, J. Blaise, A. Collin, Experimental investigation of radiation transmission through a water spray, J. Quant. Spect. Rad. Tran. 97 (2006) 126–141.
[8] P. Boulet, A. Collin, G. Parent, Heat transfer through a water spray curtain under the effect of a strong radiative source, Fire Safety J. 41 (2006) 15–30.
[9] G. Grant, J. Brenton, D. Drysdale, Fire suppression by water sprays, Progr. Energy Combust. Sci. 26 (2000) 79–130.
[10] J.F. Sacadura, Radiative heat transfer in fire safety science, J. Quant. Spect. Rad. Tran. 93 (1) (2005) 5–24.
[11] B. Oesterlé, A. Petitjean, Simulation of particle-to-particle interactions in gas–solid flows, Int. J. Multiphase Flow 19 (1993) 199–211.
[12] S. Moissette, B. Oesterlé, P. Boulet, Temperature fluctuations of discrete particles in a homogeneous turbulent flow: a Lagrangian model, Int. J. Heat Fluid Flow 22 (2001) 220–226.
[13] P. Boulet, S. Moissette, Influence of the particle-turbulence modulation modelling in the simulation of a non-isothermal gas–solid flow, Int. J. Heat Mass Transfer 45 (2002) 4201–4216.
[14] M. Rüger, S. Hohmann, M. Sommerfeld, G. Kohnen, Euler/Lagrange calculation of turbulent sprays the effect of droplet collisions and coalescence, Atomization Sprays 10 (2000) 47–81.
[15] G. Kohnen, M. Rüger, M. Sommerfeld, Convergence behaviour for numerical calculations by Euler/Lagrange method for strongly coupled phases, in: Proceedings of the Fed. Summer Meeting of the ASME 1994, 1994, pp. 191–202.
[16] B. Abramzon, W.A. Sirignano, Droplet vaporization model for spray combustion calculations, Int. J. Heat Mass Transfer 32 (9) (1989) 1605–1618.
[17] N. Berour, D. Lacroix, P. Boulet, G. Jeandel, Radiative and conductive heat transfer in a non-grey semitransparent medium—application to fire protection curtains, J. Quant. Spect. Rad. Tran. 86 (2004) 9–30.
[18] P. Boulet, A. Collin, J.L. Consalvi, On the finite volume method and the discrete ordinates method regarding radiative heat transfer in acute forward anisotropic scattering media, J. Quant. Spect. Rad. Tran. (2006), in press, doi:10.1016/j.jqsrt.2006.09.010.
[19] L. Zimmer, Etude numérique et expérimentale de la turbulence en écoulement gaz-gouttelettes. Applications aux rideaux d'eau en présence de vent latéral, PhD thesis, Institut Von Karman et UHP Nancy 1, 2001.
[20] A. Berlemont, M.S. Grancher, G. Gouesbet, Heat and mass transfer coupling between vaporizing droplets and turbulence using a Lagrangian approach, Int. J. Heat Mass Transfer 38 (16) (1995) 3023–3034.
[21] S. Elgobashi, On predicting particle-laden turbulent flows, Appl. Sci. Res. 52 (1994) 309–329.
[22] G.M. Faeth, Current status of droplet and liquid combustion, Progr. Energy Combust. Sci. 3 (1977) 191–224.
[23] H.K. Versteeg, W. Malalasekera, An Introduction to Computational Fluid Dynamics. The Finite Volume Method, Pearson Education Limited, 1995.
[24] A. Collin, Transferts de chaleur couplés rayonnement–conduction–convection. Application à des rideaux d'eau soumis à une intense source radiative, PhD thesis, Université Henri Poincaré, Nancy 1, 2006.
[25] G.M. Hale, M.R. Querry, Optical constants of water in the 200 nm to 200 μm wavelength region, Appl. Opt. 12 (3) (1973) 555–563.
[26] A. Soufiani, J. Taine, High temperature gas radiative property parameters of statistical narrow-band model for H_2O, CO_2 and CO, and correlated-k model for H_2O and CO_2, Int. J. Heat Mass Transfer 40 (4) (1997) 987–991.
[27] M.F. Modest, Radiative Heat Transfer, international ed., McGraw-Hill, 1993.
[28] B.T. Wong, M.P. Mengüc, Comparison of Monte Carlo techniques to predict the propagation of a collimated beam in participating media, Numerical Heat Transfer Part B 42 (2002) 119–140.